BEAMING OF PLANETARY RADIO EMISSIONS

Philippe Zarka

Groupe de Radioastronomie Décamétrique, UA CNRS 324,
Observatoire de Paris, Section de Meudon, DASOP,
92195 Meudon Principal Cedex, France

Abstract

The directivity of planetary radio emissions provides, together with their emission mode and source location, a fundamental clue to their generation mechanism, which is probably the same for the four planets today known to emit intense low frequency radio radiation, i.e. the Earth, Jupiter, Saturn and Uranus.

While the terrestrial kilometric emission has been observed for many years from every possible direction in space, allowing reliable statistical studies of its beaming pattern, only small portions of the 4πsr sphere around Jupiter and Saturn have been explored by Voyager 1 and 2 spacecraft (and also by ground–based radiotelescopes in the case of Jupiter's decametric emission). However, indirect techniques, including statistical and interplanetary scintillation studies for the Jovian decametric emission, and a stereoscopic study of the Saturnian kilometric radiation, have been used to obtain information on the instantaneous and average beaming of these emissions. Finally, the analysis of the data recently collected by Voyager 2 near Uranus brought direct information on the emission lobe of the Uranian kilometric emission: due to the 60° tilt of Uranus' magnetic dipole relative to its rotation axis, a large range of magnetic latitudes was explored by the spacecraft during the encounter.

The results concerning the instantaneous and average directivity of these four planetary radio emissions are reviewed and critically discussed; the most characteristic features of their beaming patterns are derived and compared with present theoretical knowledge on the subject, and particularly with the predictions of the Cyclotron Maser Instability theory, which is by far the most accepted and studied generation mechanism at present time. The needs for future observations and theoretical studies are finally stated.

1. Introduction

The low–frequency radio emissions from the Earth, Jupiter, Saturn and Uranus are emitted mainly in the fast extraordinary magnetoionic (X) mode, and their source locations, which have been determined by various methods, are now known to lie in the auroral regions of these planets (see Genova, 1987b, and references therein for the Earth, Jupiter, and Saturn, and the recent investigations by Leblanc et al., 1987, Lecacheux and Ortega–Molina, 1987, and Zarka and Lecacheux, 1987, for Uranus). Knowledge of the beaming of these planetary radio emissions is however crucial for comparing the numerous existing theories (which will not be reviewed exhaustively here) proposed for the generation of these emissions.

This paper reviews the most significant results of the observational studies of the beaming patterns of the four emissions, and compares them with theoretical predictions. Evidences are presented which favour hollow–beam or two–beam patterns for the radio emissions from the Earth, Jupiter, Saturn and Uranus.

2. Earth's auroral kilometric radiation

From a study of 5 years of electric field data, recorded with the Plasma Wave experiment aboard Hawkeye 1 and Imp 6 spacecraft from observing distances between ≤ 3 and ~ 33 Earth radii, Gallagher and Gurnett (1979) determined an average location and beaming pattern for the source of AKR at 178, 100 and 56.2 kHz (displayed in Figure 1). The northern and southern sources are on the nightside of the planet. The AKR emission cone was found to decrease with frequency. Due to reflection of radio waves at the denser plasmasphere, the emissions are visible from nightside equatorial regions only beyond $\sim$ 12 Earth radii, while the dayside polar cups are illuminated at distances as close as 4 radii.

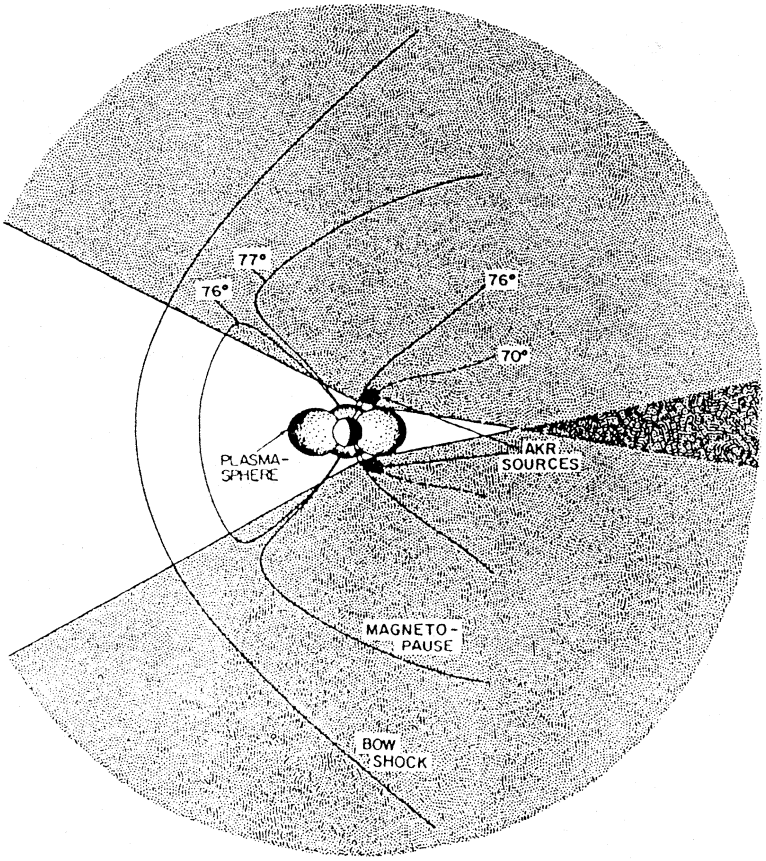

Fig. 1 (from Gallagher and Gurnett, 1979): Time–averaged extent of the conelike emission of auroral kilometric radiation from the Earth (shaded).

Green and Gallagher (1985) refined these results by studying the detailed intensity distribution of the AKR emission cone at the above frequencies. Source–centered beaming patterns at 100 and 56.2 kHz are displayed in Figure 2, with solid angles of 3.3 and 2.7 sr., respectively. The time–averaged intensity received from large radial distances over the north polar regions is plotted in a magnetic reference frame (with z–axis parallel to the Earth's dipole) centered on the source region. The authors presented these results as evidence of a wide filled emission pattern.

However, Calvert (1987a) showed that, at 56.2 kHz and possibly at 100 kHz, the measured AKR pattern was consistent with a two–beam pattern, with hollowness in the direction of the B–field and its gradient B in the source region. This hollowness is identified to the pronounced minimum of the average AKR intensity at 30° to 45° latitude, spanning the entire evening sector and splitting the pattern into separate polar and equatorial lobes (Figure 2).

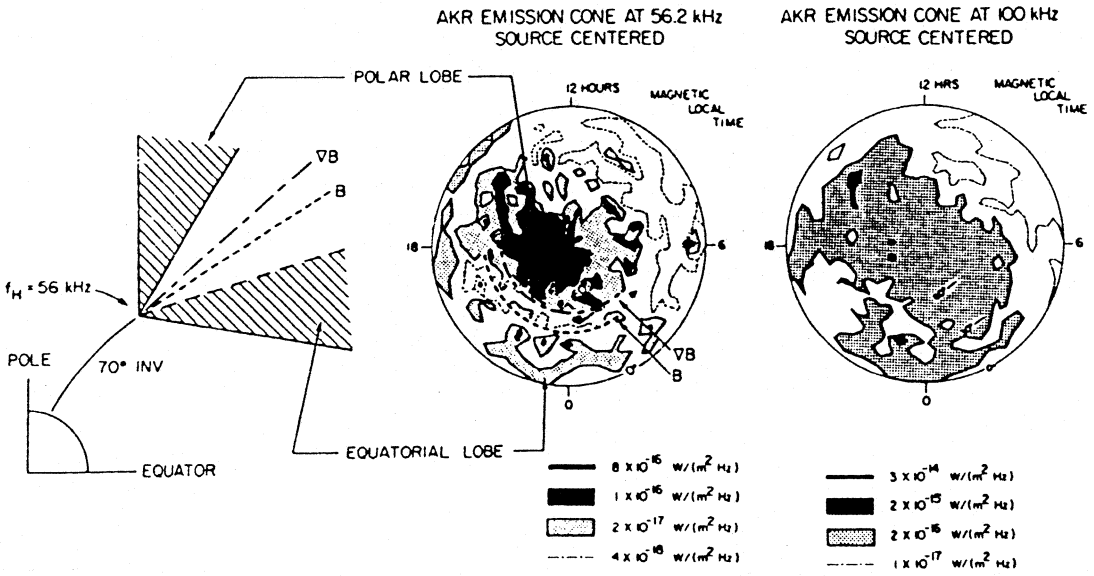

Fig. 2 (adapted from Green and Gallagher, 1985; and from Calvert, 1987a): Source centered AKR emission cones at 56.2 and 100 kHz (center and right), and their interpretation as a two beam pattern with hollowness in the direction of the B–field and its gradient in the source region (left).

From simultaneous variations of AKR intensity measured while both spacecraft were in the average emission lobe (Figure 3), Green and Gallagher (1985) also concluded that the AKR instantaneous emission pattern was a wide filled conical beam uniformly illuminated. However, Zarka and Pedersen (1986b) pointed out the fact that differences (apparently uncorrelated) as large as 10 to 20 dB exist between the two curves of the measured fluxes, in either sense (Figure 3a). These authors also computed linear cross–correlation coefficients (C) of the two curves, over a constant number (17) of consecutive data points. C$\sim$1 was obtained for 20 min. time–averaged data points, while values as low as C$\sim$0.3 (no significant correlation) were found by cross–correlating 17 consecutive 5 min–time–averaged data points of each curve.

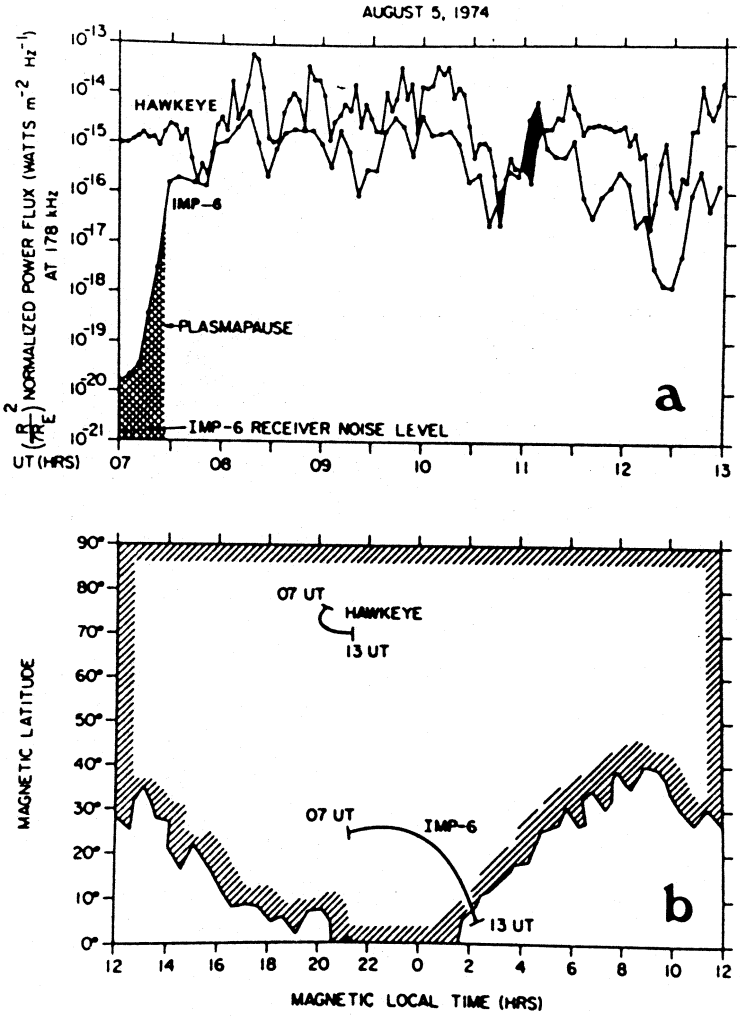

Fig. 3 (from Green and Gallagher, 1985): Simultaneous AKR power flux measurements at 178 kHz from Hawkeye and Imp 6 (a), done while both spacecraft were in the average emission lobe at this frequency (b).

From the above results, one has to conclude that the instantaneous AKR emission lobe is narrow (otherwise ∼1 to 1 correlation of intensity fluctuations would exist between the two spacecraft measurements). However, this narrow lobe probably fluctuates with time, as it statistically fills (on the average) a large emission cone in a characteristic time ≥ 20 minutes. The same conclusions are obtained in Saturn's case (see Section 4).

3. Jovian decameter and hectometer emissions

For Jupiter, the situation is more intricate due to the much more complex phenomenology of the emission, mainly related to the presence of Io. However, many independent studies show evidence for hollow cone patterns for the Io–controlled as well as Io–independent emissions (see also the review by A. Boischot, this book).

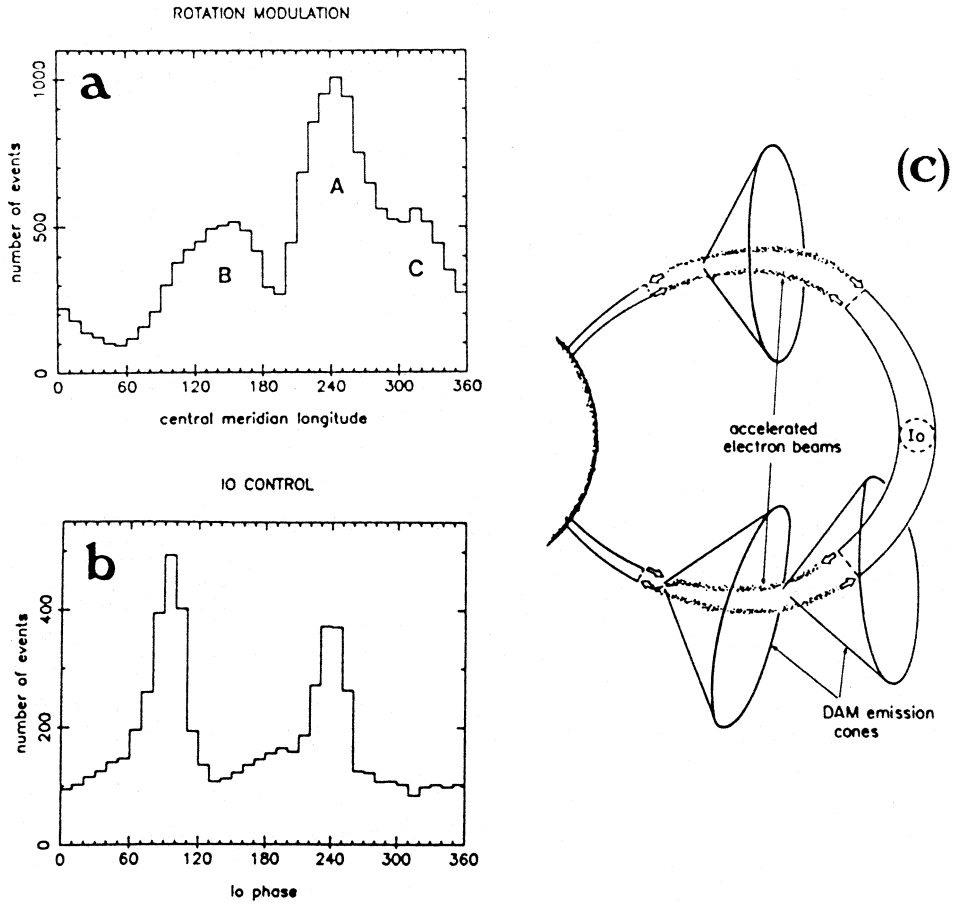

Fig. 4 ((a) and (b) from Genova et al., 1988; (c) adapted from Goldstein and Goertz, 1983): Occurrence of Jovian DAM versus observer's longitude (CML) (a) and Io–phase (b), and schematic interpretation in terms of emission beaming in hollow cones (c).

The two–lobed pattern of DAM occurrence versus observer's longitude (CML) (see Figure 4a, where are also indicated the usual names of Io–DAM "sources") and Io–phase (Figure 4b) are interpreted as the viewing of the two sides of a unique sharply beamed conical emission lobe, behaving like a corotating "searchlight beam". Its semi–apical angle, $\sim 70°$ – $80°$, has been estimated by the following different approaches:

1. Direct interpretation of the observed patterns (Dulk, 1967; Genova and Aubier, 1985), the Io–DAM being assumed to be generated by electron acceleration in or near the Io flux tube (as sketched in Figure 4c).

2. Correlations of simultaneous observations recorded from different directions (Earth–based radiotelescopes and spacecraft radioastronomy receivers) (Poquerusse and Lecacheux, 1978; Maeda and Carr, 1984; Riihimaa, 1986). In particular, Maeda and Carr (1984) found a significant correlation with $\sim$42 min–lag between DAM emission observed from Voyager 1 and the Earth. They interpreted it in terms of different declinations of the observer relative to the DAM searchlight–like beam, and put constraints on the beam shape.

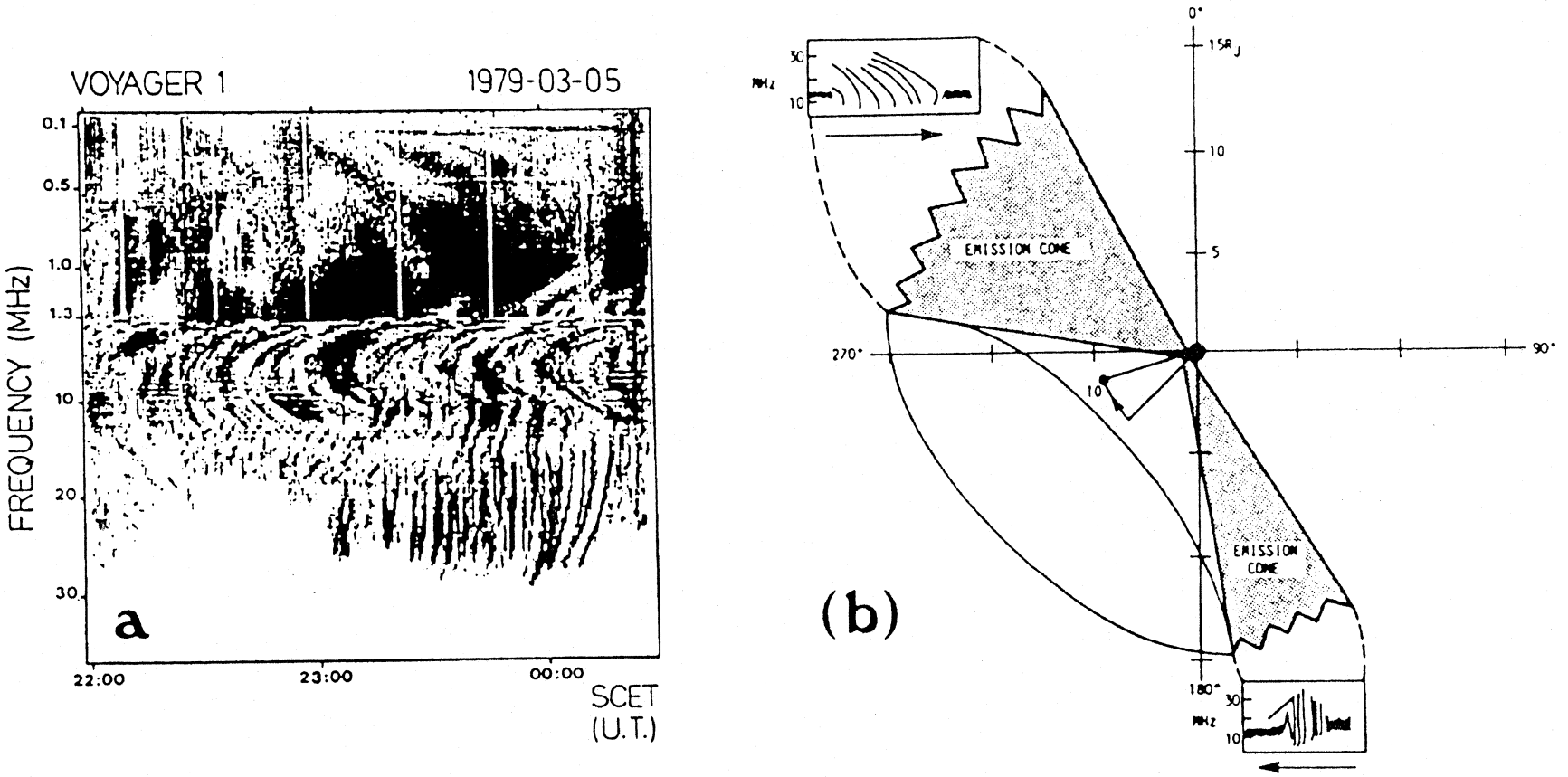

Fig. 5 ((a) from Genova et al., 1988; (b) from Green, 1984): (a) Arc structures commonly observed by Voyager in the dynamic spectra of Jupiter decameter emission. Increasing darkness corresponds to increasing intensity. (b) Sketch of the modelling of these arc structures together with the occurrence of Io emissions, through ray tracing, in terms of a hollow cone moving along with Io.

3. Ray tracing calculations (Menietti et al., 1984b; Green, 1984). This last author modelled the arc structure (Figure 5a) and occurrence of Io emissions in terms of a hollow conical sheet moving along with Io, with an edge about 30° broad (Figure 5b).

4. Interplanetary scintillation studies. The propagation of DAM through inhomogeneities convected in the solar wind produces drifting features in the dynamic spectra (Figure 6). The existence of measurable drifts proves that the source is spatially spreaded along field lines, and that the emission occurs at wide angle from the magnetic field in the source. The sense of the drifts, which reverses for A and B sources (either Io or non–Io) indicates that they are seen resp. near the West and East limbs of the planet (see Genova and Boischot, 1981; and Boischot et al., 1987; among others).

5. Theoretical considerations. For example, Hewitt et al. (1981) showed that the cyclotron maser theory applied to DAM generation leads naturally to a prediction of emission concentrated on a thin, widely open hollow cone. Goldstein and Goertz (1983) obtained the same result in the frame of the 3–waves up–conversion mechanism.

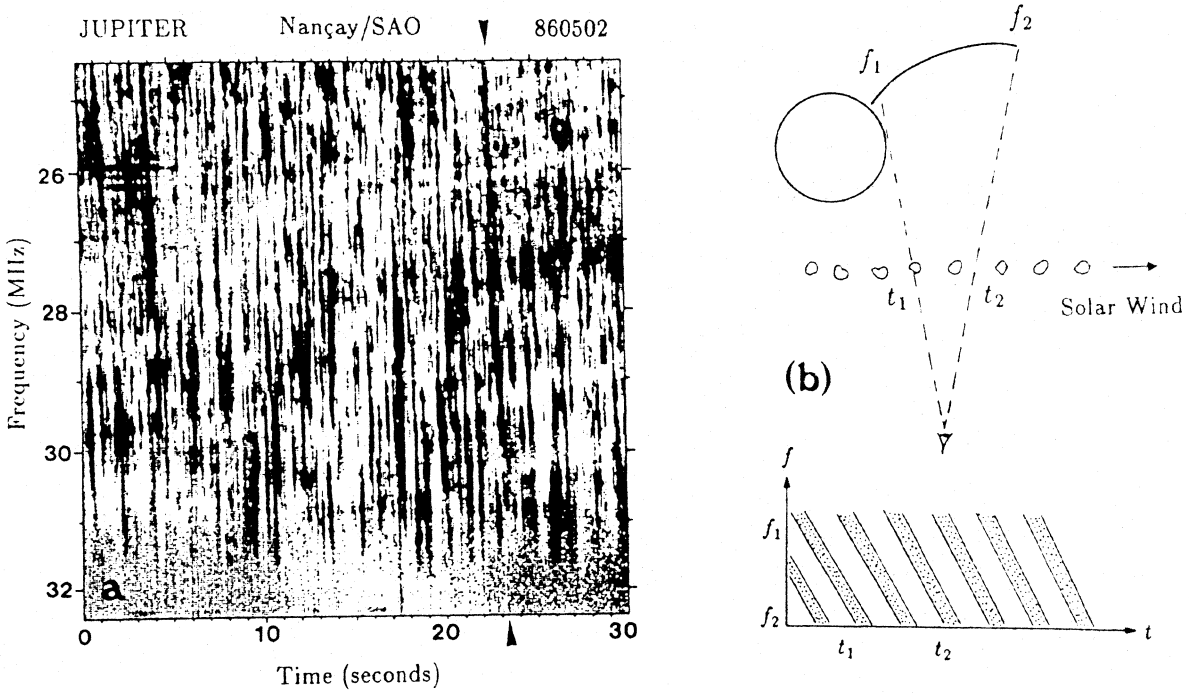

Fig. 6: (a) Dynamic spectrum of Jovian emission obtained by the Acousto– Optical Spectrograph operating in Nançay. For a source spatially distributed as a function of the frequency, the interplanetary scintillation produces drifting features in the dynamic spectra (indicated by the arrows), as sketched in (b).

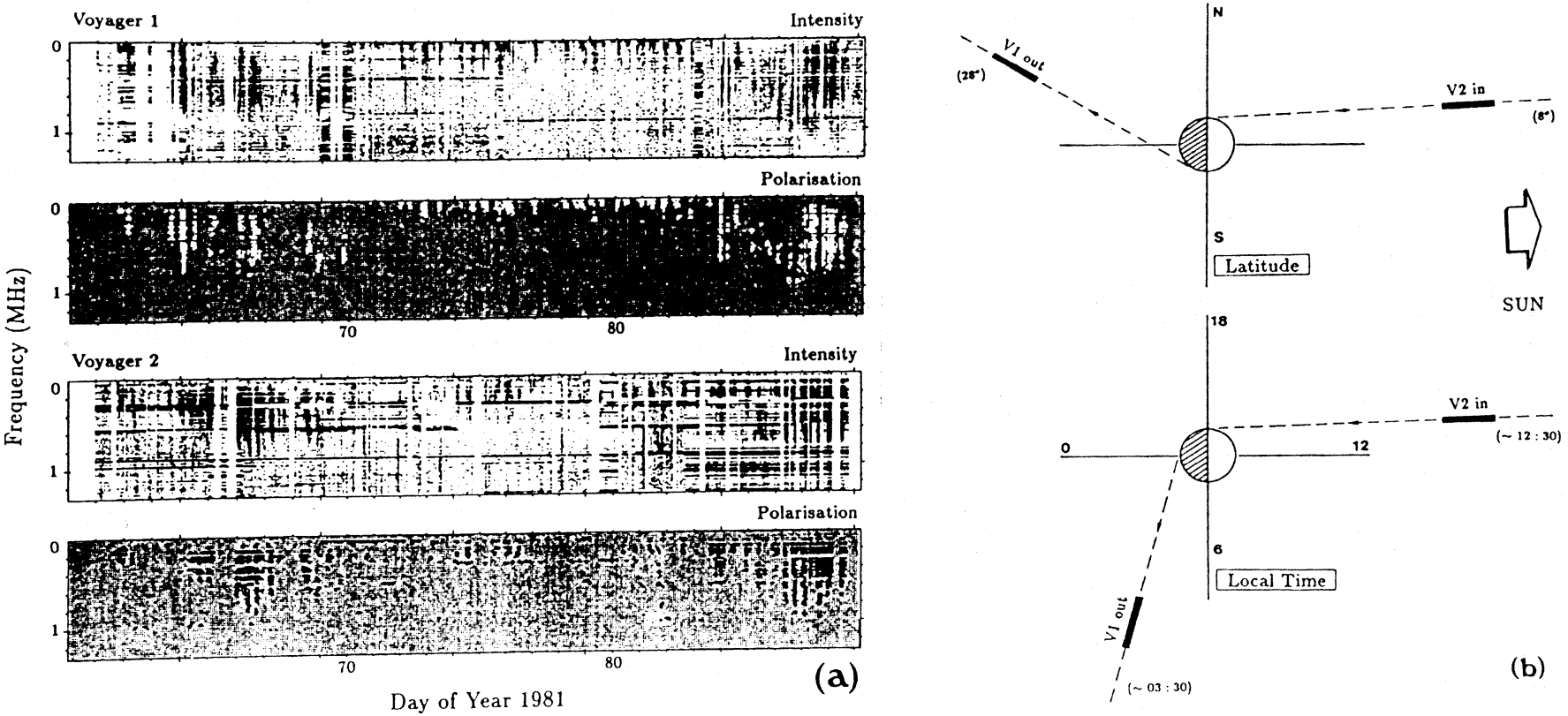

Fig. 7: (a) Compressed dynamic spectra of SKR intensity (in grey levels) and observed circular polarization sense (white=LH, black=RH). The observing geometry, very different for Voyager 1 and 2, corresponding to the ~1 month–data–interval studied (thick lines), is represented in (b). The long–term fluctuations of the emission observed by both spacecraft seem correlated.

Moreover, dramatic changes in DAM occurrence and HOM morphology as a function of the observer's Jovigraphic latitude, which varies only by ±3.3° during the Jovian year, support a strong latitudinal beaming of these emissions (Lecacheux, 1974; Alexander et al., 1979b). The conical sheet on which they occur is generally found to be narrow (a few degrees) except for Green (1984). The millisecond emission (S–bursts) seems even more sharply beamed (Genova and Calvert, 1988).

4. Saturnian kilometric radio emission

Large intensity and frequency range fluctuations are observed on dynamic spectra of SKR, on different timescales ($\leq$ 1 s to several days). These fluctuations seem long–term correlated, as observed stereoscopically by Voyager 1 and 2 spacecraft from different positions in local time and latitude (see Figure 7). Therefore on shorter timescales, the emission looks different on the two spacecraft (Figure 8).

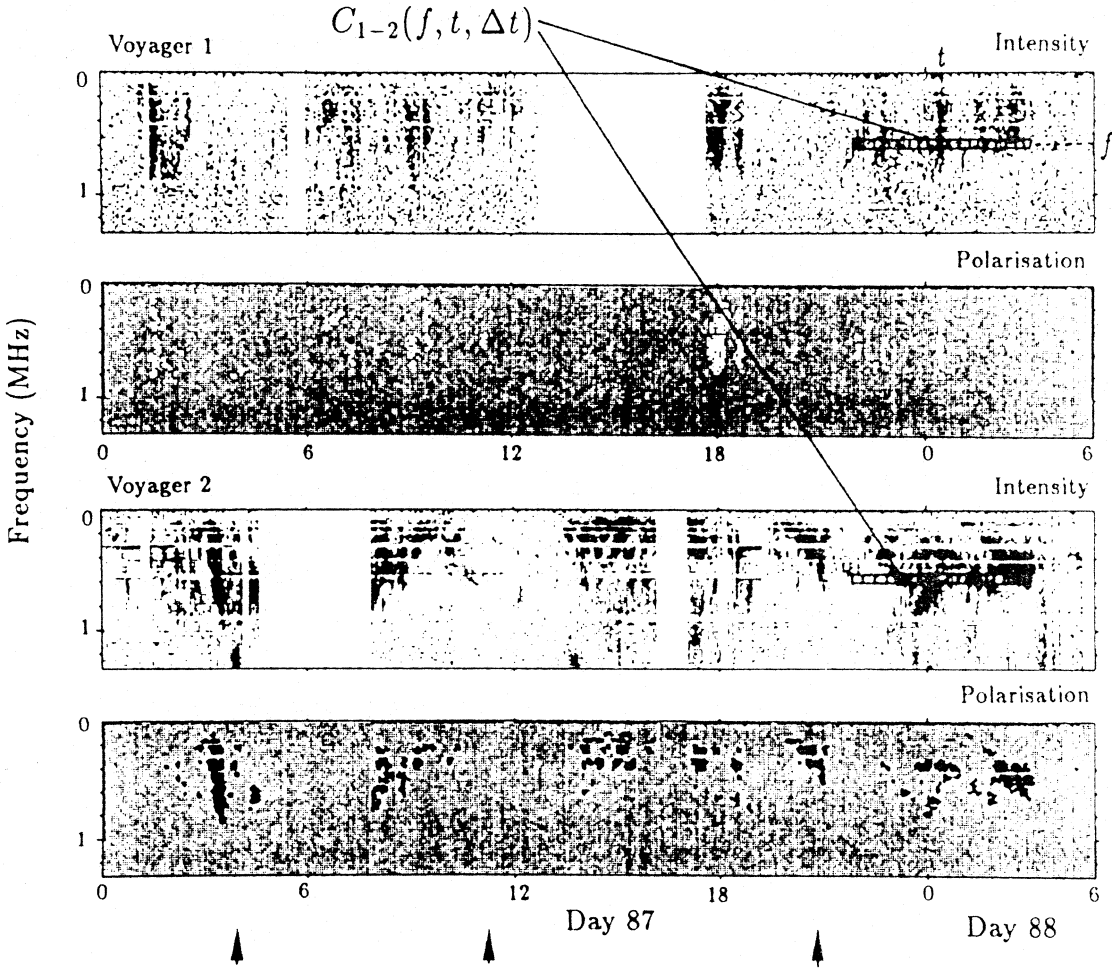

Fig. 8: Expanded dynamic spectra of SKR, under the same format as Figure 7a. 30 hours of data are displayed here, together with a sketch explaining the calculation of the linear correlation coefficient $C_{1-2}(f,t,\Delta t)$ (see text). The arrows point out uncorrelated events for which SKR is observed by one spacecraft only.

Zarka and Pedersen (1986b) have calculated linear cross–correlation coefficients (computed over samples of n=40 points) between the fluxes measured by Voyager 1 and 2 as a function of:

- frequency
- interval Δt of flux–averaging for each data point
- time t of the center of the $n \times \Delta t$ data interval used in the computation of the coefficient $C_{1-2}(f, t, \Delta t)$ (as illustrated in Figure 8).

Their results are summarized in Figure 9. When displaying the value of C_{1-2} in grey levels as a function of time and frequency (black: C=1; white: C=0), the flux measured simultaneously by the two Voyagers appears uncorrelated at all frequencies for a time–averaging $\Delta t \leq 10$ min (Figure 9a), while for a time averaging of 1/2 Saturnian rotation ($\sim$ 5h), the correlation is good where emission exists, and reproduces then the dynamic spectrum of SKR (as it can be seen by comparing Figures 9b and 7a). Finally, the average cross–correlation coefficient is found to increase from $\sim$0 to very significant values when Δt increases from 0 to one Saturnian rotation (Figure 9c). The critical time–averaging value is about 0.5–1 hour. As a check, the same work done before Voyager 1 and 2 encounters, when both spacecraft were in very close directions in space, leads to a very good correlation at all timescales.

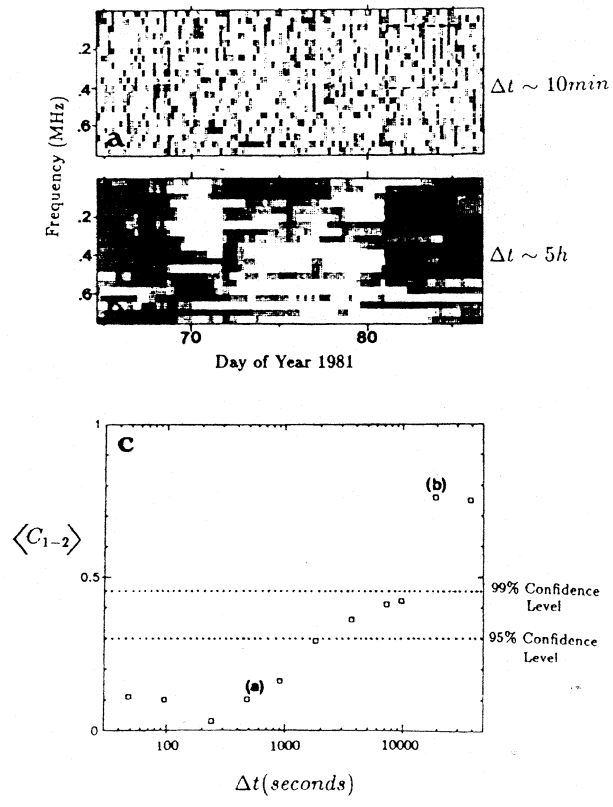

Fig. 9: Correlation coefficient C_{1-2} as a function of time and frequency, displayed in grey levels (black: C_{1-2} = 1, white C_{1-2} = 0), (a) for a time–averaging $\Delta t \sim$ 10 min, and (b) for a time averaging of half a Saturnian rotation ($\sim$5h). (c) Correlation coefficient C_{1-2} averaged over the dashed region of Figures (a) and (b) for Δt = 48s to one Saturnian rotation ($\sim$10h 40min).

Thus it can be concluded that the SKR instantaneous radiation pattern is narrow beamed. But, it fills statistically a large emission lobe in characteristic times about 0.5 to 1 hour. As a consequence, the source location proposed by Kaiser and Desch (1982) (black region of Figure 10), based on comparisons of SKR intensities before and after encounter modelled by a wide beam in $\cos^n(\theta)$, appears very questionable. We tend to prefer the less accurate but more founded method of Lecacheux and Genova (1983), assuming only an average wide (half–space) beam occulted by the planet (and leading to the hatched region of Figure 10).

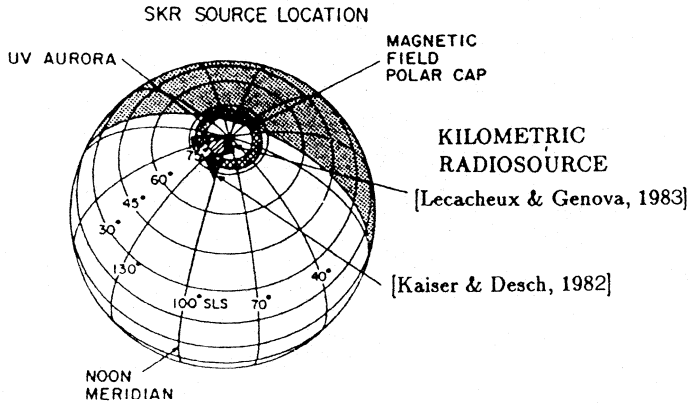

Fig. 10 (adapted from Kaiser et al., 1984): Best estimates for the northern source footprints of SKR, as determined by Kaiser and Desch (1982) (black) and Lecacheux and Genova (1983) (hatched).

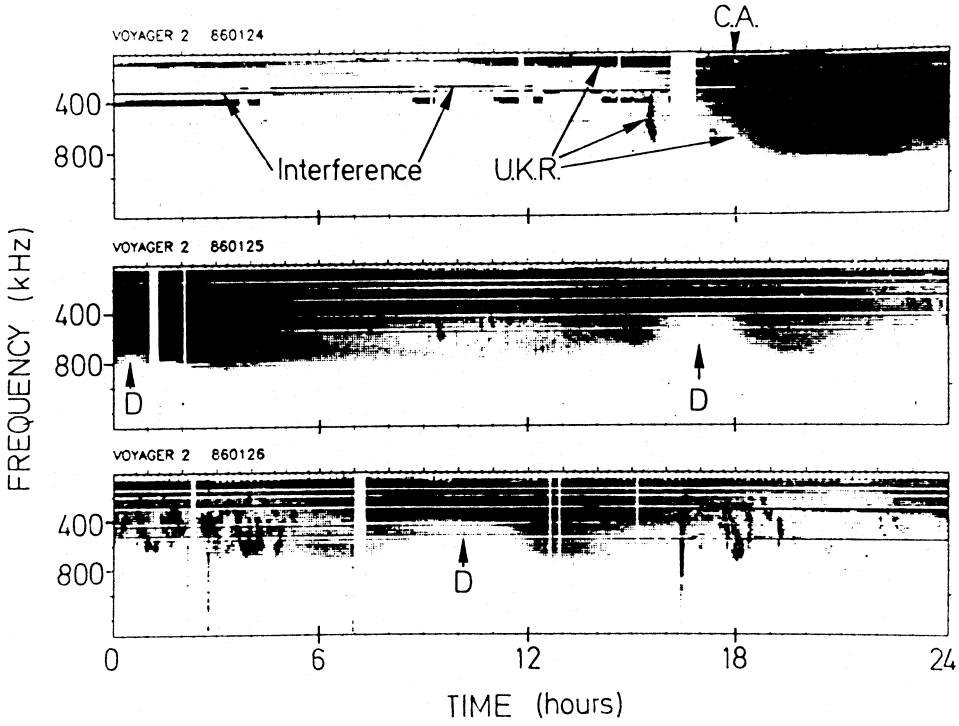

Fig. 11 (from Zarka and Lecacheux, 1987): Dynamic spectra of UKR recorded by Voyager 2 for 3 days around closest approach. The prominent post–encounter broadband emission consists of a smooth, slowly varying component over which is superimposed a bursty emission. Intensity dropouts (D) affect the high frequency part of the emission on each rotation (i.e. 17.24h interval).

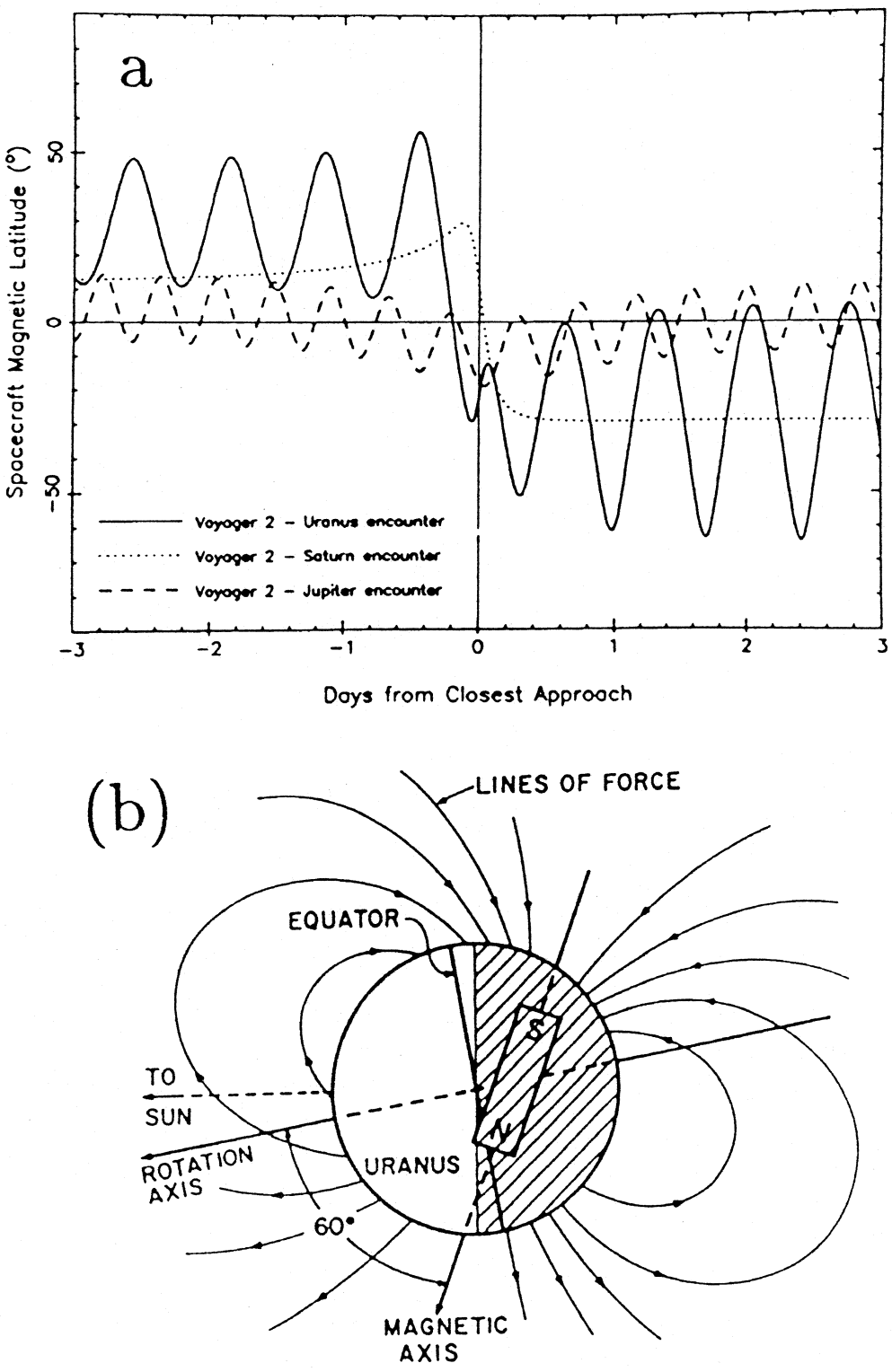

Fig. 12 ((a) from Zarka and Lecacheux, 1987; (b) from Ness et al., 1986): (a) Magnetic latitude of Voyager 2 relative to the Uranian, Saturnian, and Jovian dipole fields, for 3 days before and after closest approach to the planet. The latitude ranges explored by the spacecraft are much wider for the encounter with Uranus, due to the large tilt of the Uranian dipole relative to the rotation axis of this planet (b).

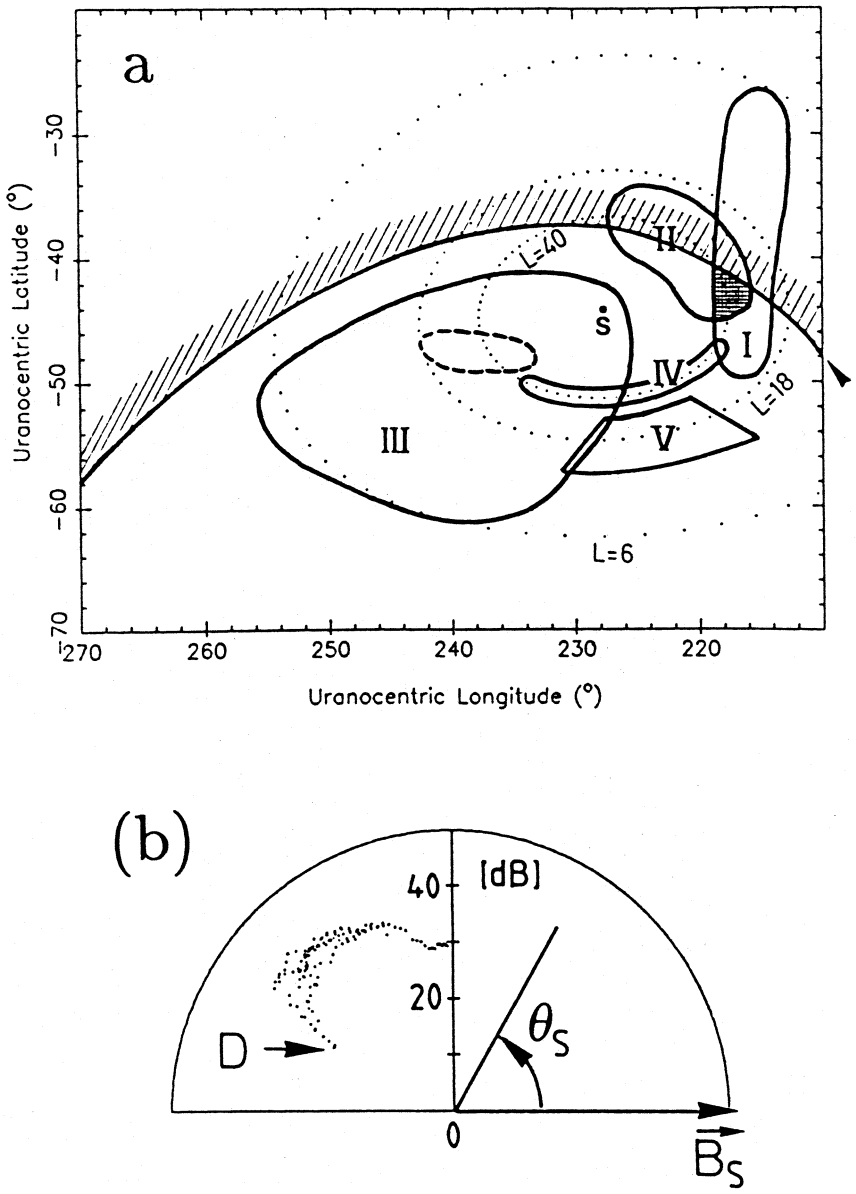

Fig. 13 (from Zarka and Lecacheux, 1987): (a) Comparison of source locations obtained by several authors for the UKR nightside component (see text). S is the southern OTD dipole tip. For a source footprint taken in the cross–hatched region, the corresponding UKR pattern at ∼600 KHz is displayed in (b) in polar coordinates relative to the magnetic field direction in the source region (B_S).

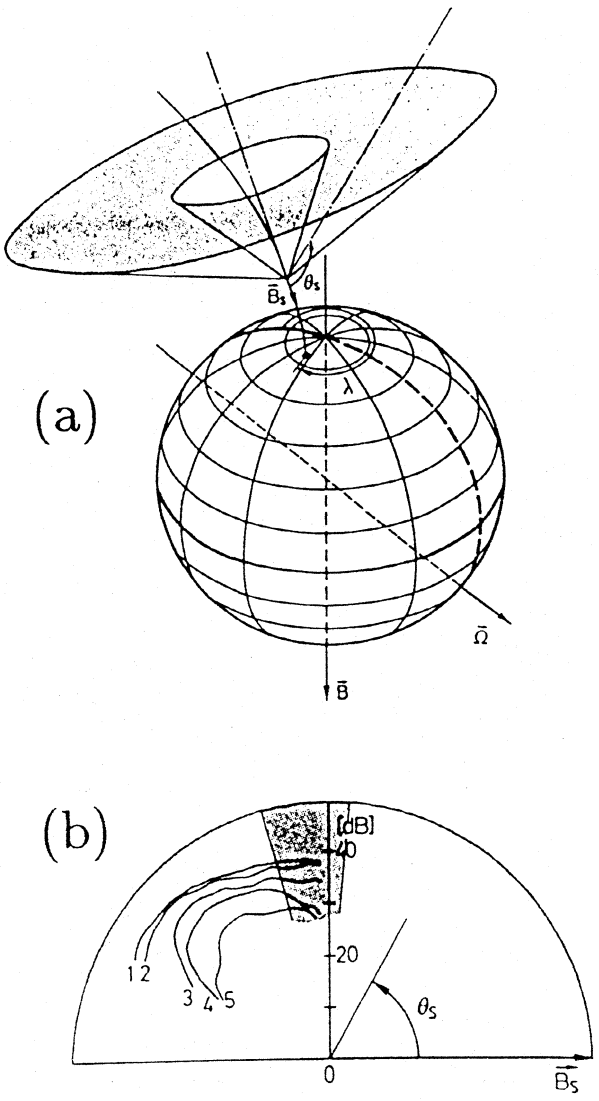

Fig. 14 (from Zarka and Lecacheux, 1987): (a) Schematic sketch of the UKR beaming (for a frequency ∼600 kHz). It is a hollow cone with ∼ 100° aperture and 40° angular thickness, directed outwards from the planet. Cuts of this emission lobe by a magnetic meridian half–plane are displayed in (b) for different frequencies: (1) 154.8 kHz, (2) 346.8 kHz, (3) 462.0 kHz, (4) 596.4 kHz, and (5) 750.0 kHz. The bursty component is beamed over the grey–shaded zone, towards the local magnetic equator.

5. Uranus kilometric radiation

Figure 11 shows typical dynamic spectra of UKR. As for the three other planets, the post–encounter broad–band emission (studied here) is emitted in the X–mode. Uranus is the only planet other than the Earth whose radio emission beaming pattern has been determined directly from observations. The larger range of magnetic latitudes explored by Voyager 2 during its encounter with Uranus, about 120° compared to 20° – 40° in the case of Jupiter and Saturn (see Figure 12a), allowed a direct investigation of its radio lobe. This was possible due to the large tilt of the Uranian magnetic dipole relative to the rotation axis of this planet (Figure 12b displays the OTD model of Ness et al., 1986).

Several authors constrained the source location of the broadbanded UKR to the southern (nightside) auroral region of the planet (Zarka and Lecacheux, 1987 region (I) of Figure 13a; Lecacheux and Ortega–Molina, 1987, (II); Leblanc et al., 1987. (III); Gulkis and Carr, 1987, (IV); and Kaiser et al., 1987, (V)). This allowed (Zarka and Lecacheux, 1987) to plot the UKR intensity (measured at 600 kHz, during day 24, 22:00 to day 26, 12:00) versus angle θ_S between the spacecraft direction as seen from the source (assumed to lie on a small set of L=40 field lines), and the magnetic field in the source B_S (Figure 13b). The true emission pattern results approximately from cylindrical symmetry of this diagram around B_S, and is thus a hollow cone (see Figure 14a). The time–averaged source–centered UKR beaming pattern is also given at 5 frequencies in Figure 14b: (1) 150 kHz, (2) 350 kHz, (3) 460 kHz, (4) 600 kHz, and (5) 750 kHz; it broadens with decreasing frequency. The observed dropouts (D) correspond to Voyager's trajectory crossing the hole of the emission cone. The bursty component of the UKR emission is emitted over the grey–shaded region.

Gulkis and Carr (1987) obtained comparable results from a different approach: modelling the observed UKR intensity variations by a $\cos[n(\theta - \theta_0)]$ beam, emanating from the southern auroral arc observed at UV wavelengths by Voyager, they found an average emission cone with 100° – 120° aperture and 20° – 40° thickness. Obviously, for all planets, the instantaneous emission pattern could be a much thinner conical sheet than the time–averaged one.

6. Conclusions

From the above review, it appears that a hollow conical beam is probably the common average beaming pattern of the radio emissions from the Earth, Jupiter, Saturn and Uranus. Among the currently existing generation mechanisms, the most studied (and seemingly the most relevant) is certainly the Maser Synchrotron Instability (MSI, also called cyclotron maser instability). This mechanism naturally predicts wave amplification (and hence substantial emission) only in a narrow range of angles (a few degrees) almost perpendicularly to the magnetic field in the source regions (the precise values depending on the local magneto–plasma parameters). For the Earth, Zarka et al. (1986) found an optimal emission range of 74° – 76°. However, the MSI has also been successfully applied to the Jovian DAM (Hewitt et al., 1981), to the SKR (by Galopeau et al., 1988; with

a predicted wave normal angle at $\sim 85°$ from the direction of B_s over the major part of the spectrum), and to the UKR (by Gulkis and Carr (1987), as a frame of their lobe modelling).

Comparable theoretical developments are needed for the other candidate generation mechanisms. In addition, the MSI itself needs to be further investigated, especially in an attempt to clarify its role in the short–term fluctuations of the emissions. This is particularly important concerning their directivity, as the instantaneous emission lobe (at least for the Earth, Jupiter and Saturn) seems to be a much narrower beam than the time–averaged one. This could also be due to fluctuation of magnetic field line geometry, of the location of particle precipitation, or due to propagation effects in or close to the source region, causing a displacement or flickering of the instantaneous beam in space (and possibly related to fluctuations of the solar wind parameters – ram pressure, for example – at the planet). These questions have to be studied in the frame of global magnetospheric dynamics and its link to the microscopic phenomena occurring in the auroral regions of the magnetized planets, such as the generation of radio waves.

An invaluable input to the problem has been obtained for the Earth by the Viking spacecraft, in terms of observations of radio waves in their source region, together with hot and cold plasma distribution measurements. For Jupiter and Saturn, the Galileo and Cassini spacecraft should allow long term continuous radio observations from various directions (eventually simultaneous with solar wind measurements), and provide (indirectly) a better knowledge of the magnetic field geometry and plasma content of the radio source regions. Moreover, stereoscopic observations of DAM will be performed during the Galileo mission with the Nançay decameter array (within the frame of the International Jupiter Watch). Finally, new magnetospheric emission, from Neptune, may eventually be observed in 1989 with Voyager 2, allowing then additional interesting comparative studies of the planetary radio emissions.